Electronic Supplementary Information (ESI)

Anion-Driven Supramolecular Gel: Naked-Eye Detection of Picric Acid, Facilitating *in situ* Formation of Gel Nanocomposites and Enabling Solid-State Anion Exchange

Rubi Moral, Oiyao Appun Pegu and Gopal Das*
Department of Chemistry, Indian Institute of Technology Guwahati, Assam, 781039, India;
Email: gdas@iitg.ac.in

S1. General Information and Materials. All the reagents for synthesis were purchased from Sigma-Aldrich Chemical Co. and used without further purification. A PerkinElmer Lambda-25 UV−vis spectrophotometer was used for the measurement of the absorption spectra in the wavelength range of 250−800 nm, using 10 mm path-length quartz cuvettes. All the mass spectra were recorded using a Waters Q-ToF Premier mass spectrometer. Bruker Advance 600 MHz and 400MHz instruments were used to record Nuclear magnetic resonance (NMR) spectra, where the chemical shifts were recorded in parts per million (ppm) scale. To describe the spin multiplicities in the ^{1}H NMR spectra following abbreviations have been used: singlet: s; doublet: d; triplet: t, quartet: q, and multiplet: m. The morphology of the aggregated species was investigated by using FESEM imaging studies using Sigma 300 FESEM (10000KX).

S2. Rheological Experimental Details. Measurements were performed using a Thermo Scientific Rheometer (HAAKE MARS iQ Air) equipped with a 35 mm parallel plate arrangement. Experiments were carried out on freshly prepared gel of **GUA-IND** with $(TBA)_2SO_4$ (**GI-G**, 5 mg mL^{-1}). Linear viscoelastic regions of the samples were determined by measuring the storage modulus, G′ (associated with energy storage), and the loss modulus G″ (associated with the loss of energy) as a function of the stress amplitude. The gel-sol transitions were monitored over different shear strains with a fixed frequency at 1 Hz. As the storage modulus(G′) starts to decrease after a 1% shear strain, we decided on a shear strain of 0.1 % to measure the frequency-dependent rheological behaviors of the gels.

S3. Synthesis of GUA. GUA was synthesized using the procedure described in previous literature.[1] Guanidinium chloride (20 mmol, 1.911 g) was placed in a 250 ml round-bottom flask and dissolved in 50 ml 1,4-dioxane. An excess of hydrazine monohydrate (150 mmol, 7.3 ml) was added to it while stirring. The reaction mixture was heated at 110 °C for 3 hours under refluxing conditions. After 3 hours, the reaction mixture was cooled to room temperature, and the solid precipitate was filtered and washed with 1,4-dioxane and then dried in a vacuum desiccator. The yield obtained was ~ 98%.

S4. Synthesis of GUA-IND. GUA (1g, 237.1 mM, 1 equiv.) was placed in a 250 mL round-bottomed flask and dissolved in ethanol (EtOH) (30 mL). Indole-3-carboxaldehyde (4.6g, 2.80 mmol, 3.5 equiv.) was added, and the reaction was refluxed at 74℃ for 12 hours. The precipitates were separated by filtration and washed with EtOH (30 mL). The obtained pale-yellow amorphous product was further vacuum-dried and isolated as compound **GUA-IND**. It was further crystallized from DMSO, and a suitable single crystal was isolated for SC-XRD analysis. Calculated yield: 85%. ^{1}H NMR (600 MHz, DMSO-d_6) δ 11.95 (s, 3H), 11.34 (s, 3H), 8.88 (s, 3H), 8.42 (d, J = 7.4 Hz, 3H), 8.08 (d, J = 2.8 Hz, 3H), 7.52 (d, J = 7.4 Hz, 3H), 7.30-7.24 (m, 6H). 13C NMR (151 MHz, DMSO-d6) δ 148.71, 3×[148.10, 137.61, 132.63, 124.64, 123.34, 122.68, 121.31, 112.49, 111.07]. ESI-MS (positive mode, m/z) calculated for $C28H24N9^{+}$: 486.2149, found: 486.2172. FT-IR spectra (KBr pellet used): 3514 cm^{-1} vs (Indole N-H), 3314 cm^{-1} vs (Guanidine N-H), 3097 cm^{-1} vs (aromatic C-H), 1638 cm^{-1} (imine C=N), 1596 cm^{-1} (aromatic C=C).

S4. Synthesis of GUA-NAP. GUA (100mg, 0.71 mmol, 1 equiv.) was placed in a 250 mL round-bottomed flask and dissolved in ethanol (EtOH) (30 mL). 1-napthaldehyde (388.9mg, 2.9 mmol, 3.5 equiv.) was added, and the reaction was refluxed at 74℃ for 12 hours. The precipitates were separated by filtration and washed with EtOH (30 mL). The obtained pale-yellow amorphous product was further vacuum-dried and isolated as compound **GUA-NAP**. Calculated yield: 82%. ^{1}H NMR (600 MHz, DMSO-d6) δ 12.39 (s, 1H), 9.74 (s, 1H), 8.56 (d, J = 7.2 Hz, 1H), 8.46 (d, J = 8.5 Hz, 1H), 8.19 (d, J = 8.1 Hz, 1H), 8.10 (d, J = 8.2 Hz, 1H), 7.76 (q, J = 8.5 Hz, 3H), 7.68 (t, J = 7.4 Hz, 1H). ^{13}C NMR (151 MHz, DMSO) δ 150.19, 3×[149.55, 133.90, 132.07, 131.44, 129.49, 128.94, 128.05, 126.93, 126.70, 126.08, 123.20]. ESI-MS (positive mode, m/z) calculated for $C34H27N6^{+}$: 519.2292, found: 519.2292. FT-IR spectra (KBr pellet used): 3047 cm^{-1} vs (aromatic C-H), 1621 cm^{-1} (imine C=N), 1513 cm^{-1} (aromatic C=C).

S5. Crystallographic Refinement Details. All the details of the crystallographic refinement and hydrogen-bonding interactions are furnished in **Tables S1** and **S2,** respectively, and also all of the above-given data have been deposited into the CCDC. A suitable single crystal was selected and mounted into a loop. Supernova (a single source at an offset) Eos diffractometer with Mo Kα radiation (λ = 0.71073 Å) source, connected with a CCD region detector was used to collect the X-ray intensity data, and all the data refinement and cell reduction were done by using APEX

3/APEX 4.[2,3] Using a narrow-frame algorithm and XPREP, the frames were combined with the Bruker SAINT software kit,[4] and data were corrected for absorption effects using the Multi-Scan process (SADABS)[5]. Using direct methods in XT, version 2014/15, all of the structures were solved, and after that, refinement was done using the full-matrix least-squares technique in the SHELXL-2016 and 2018 software packages on F2.[6] MERCURY 4.2.0 was used for creating structural drawings.[7]

S6. **Field Emission Transmission Electron Microscopy (FETEM) Analysis.** CuNPs and AgNPs formation was visualised via FETEM, small portions of **GI-Cu-G** and **GI-Ag-G** gels were scooped out and smeared on carbon-coated copper grids (400 meshes) and dried in vacuum.

S7. Gel preparation. Supramolecular gels are composed of the **GUA-IND** receptor and sulfate (or bisulfate) salts (**Figure 2**). The gel **GI-G** was prepared by dissolving **GUA-IND** (5mg per ml) in DMSO, followed by rapid addition of an aqueous solution of $(TBA)_2SO_4$ salt (1 equivalent of the receptor) in a 1:4 ratio, respectively. The receptor itself cannot form a gel in the absence of the anion under the same conditions. The minimum gelling concentration for sulfate salt was found to be 0.5 equivalent of the receptor (**Figure S9**). The prepared organohydrogels were opaque, and the gelation was confirmed by the absence of flow upon vial inversion. The organogel with $(TBA)_2SO_4$ was stable up to 48-72 hours. However, the gel formed from $TBAHSO_4$ remained stable for only 3-4 hours. Various metal sulfate salts (Na^+, Mg^{2+}, Al^{3+}, K^+, Ca^{2+}, Mn^{2+}, Fe^{2+}, Fe^{3+}, Co^{2+}, Ni^{2+}, Zn^{2+}) successfully formed organohydrogels. The metal sulfate gels were stable up to 10-12 hours.

S8. PA sensing. To check the selectivity in nitro-aromatic sensing, initially we formed the **GI-G** gel in 500 μL solvent by following the initial procedure. Then we added the 3 equivalents (compared to the receptor concentration in the gel) of the nitro-aromatic compounds in the powder form on the top of the gel. Since **GI-G** could selectivity sense PA among different nitro-aromatic compounds, we then calculated the minimum amount of PA required for disruption of the gel. However, it is difficult to weigh very small amount of PA and hence to maintain the proper concentration we made PA solution (3 equivalent of the receptor concentration) in DMSO by

calculating the required amount and then diluted it to prepare 2, 1, 0.5 and 0.25 equivalent (compared to the receptor) of PA solutions. We added 100 µL of each these PA solutions on the top the **GI-G** gels prepared in different glass vials. Important to mention here that, the equivalents of PA compared to the receptor was calculated considering a total of 600 µL volume of solvent (500 µL in the gel and 100 µL for preparation of PA solution).

S9. Determination of DPPH (Radical Scavenging Assay)

2,2-diphenyl-1-picrylhydrazyl (DPPH) assay, a spectrophotometric technique, is employed for quantifying the antioxidant activity of antioxidants. The DPPH solution was prepared by dissolving in methanol (4 mg in 100 mL), and 3 mL of this deep purple coloured solution was added to 1 mL of methanolic solution of gels (**GI-G**, **GI-Cu-G,** and **GI-Ag-G**). Then these solutions were kept in the dark at room temperature for 30 min. MeOH was used for the baseline. Correction and finally, the absorbance was measured at 517 nm. The concentration of the **GI-G** gel and nanocomposite gels **GI-Cu-G** and **GI-Ag-G** were varied by pipetting out different amounts, viz. 2µL, 5µL and 7µL and then dissolved in 1ml of methanol. Radical scavenging activity was expressed as the inhibition percentage and was calculated using the following formula,

$$\text{DPPH scavenging activity (\%)} = \frac{\text{Abs}_{\text{DPPH}} - \text{Abs}_{\text{Sample}}}{\text{Abs}_{\text{DPPH}}} \times 100$$

S10. Antibacterial studies

The antibacterial performance of the organohydrogels was evaluated against gram-positive (*B. subtilis* MTCC 441) and gram-negative (*E. coli* DH5α MTCC 433) strains by the zone inhibition test.

S.10.1. Evaluation of Zone of Inhibition by Well-Diffusion Method

The antibacterial properties of the **GI-G**, **GI-Cu-G,** and **GI-Ag-G** were ascertained by the determination of the zone of inhibition by the well-diffusion method. Firstly, the respective bacterial lawn was prepared in sterile nutrient agar media plates using sterile cotton swab sticks. 10^6 CFU/ml cultures of freshly overnight-grown bacterial suspensions of representative gram-

positive (*B. subtilis*) and gram-negative (*E. coli*) bacterial strains were used to prepare the lawn culture on the plates. Following this, wells of approximately 5mm in diameter were made, and 100 µL of gel samples were added to the wells. The plates were then kept for incubation at 37 °C overnight.[8]

S11. Anion exchange study

Powder sample of **GUA-IND** was dissolved in DMSO and placed in separate vials. Different TBA salts were added to the DMSO solution of **GUA-IND** placed in individual vials and kept it undisturbed for one week. Crystals appeared in the vials were analysed and Cl^- anion of **GUA-IND** was found to be exchanged with anions like Br^-, NO_3^- and $H_2PO_4^-$ in the crystal structures.

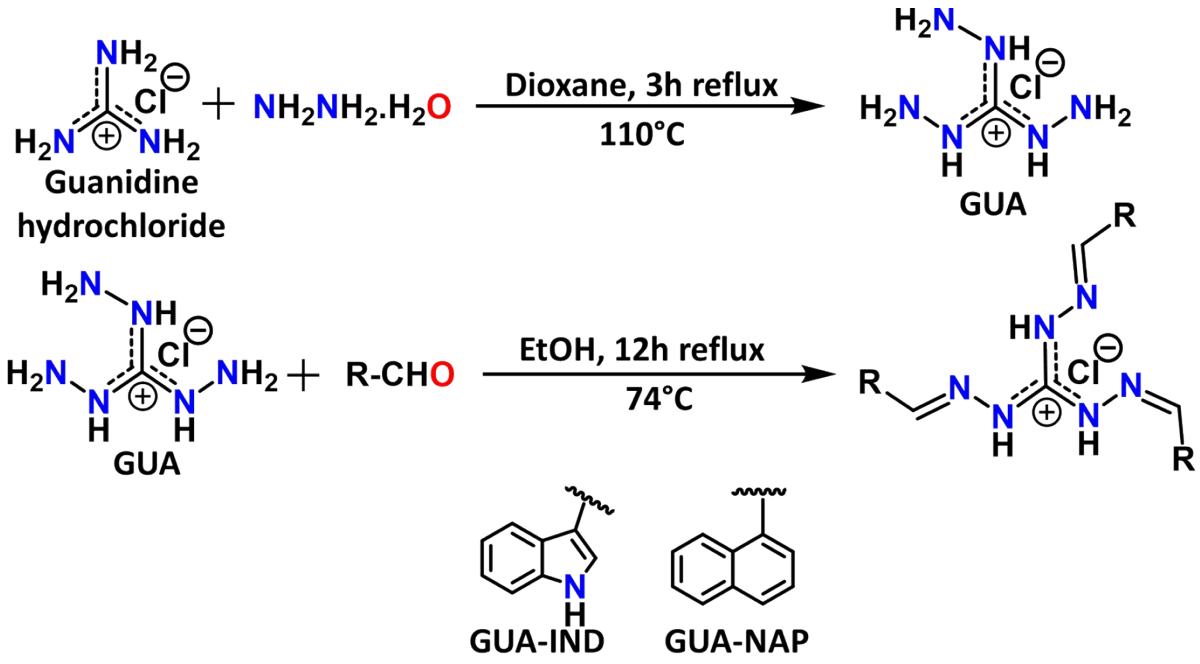

Scheme S1. Synthesis of **GUA-IND** and **GUA-NAP**.

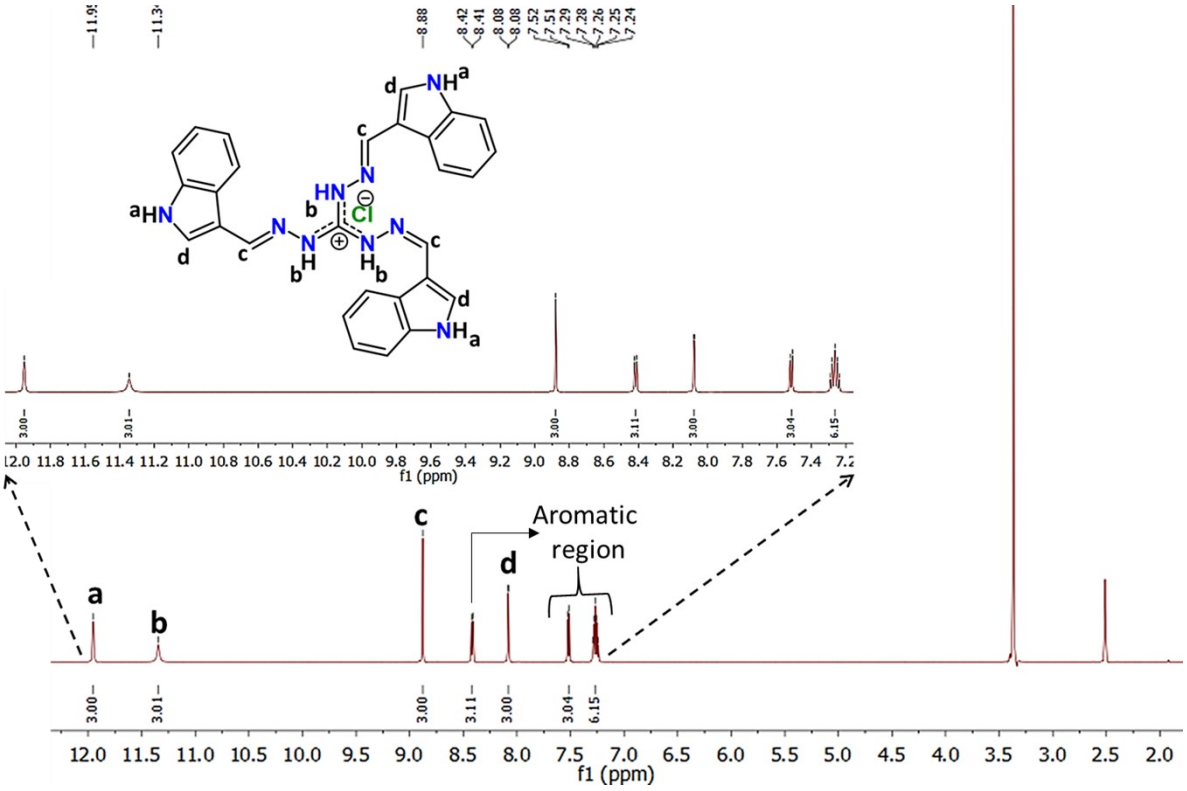

Figure S1. ^{1}H NMR spectrum of **GUA-IND** in DMSO-d_6.

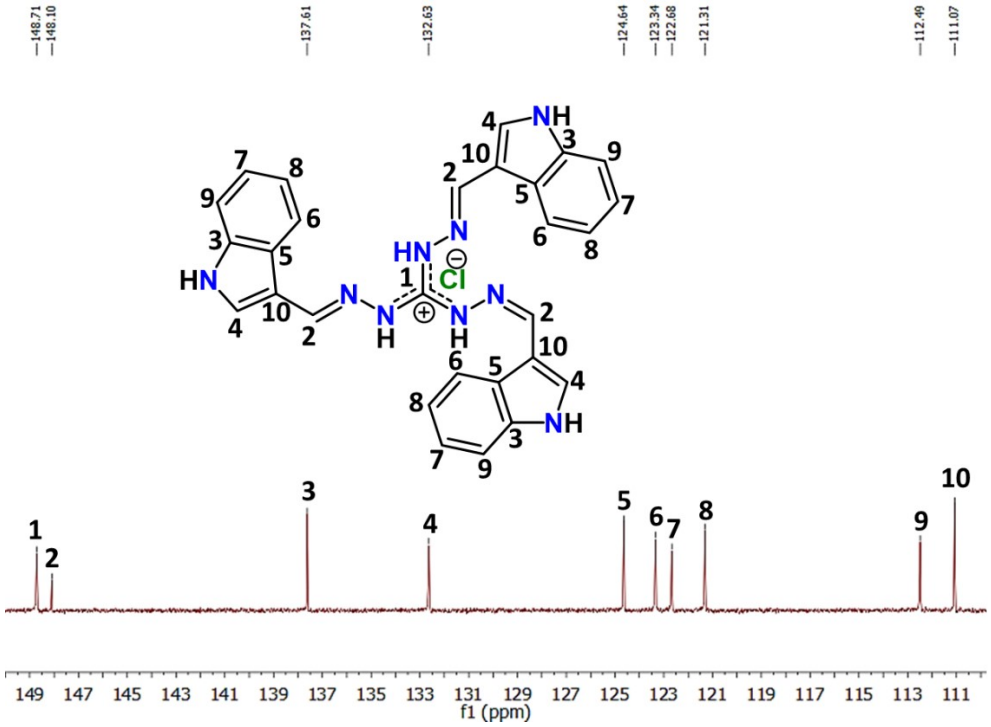

Figure S2. ^{13}C NMR spectrum of **GUA-IND** in DMSO-d_6.

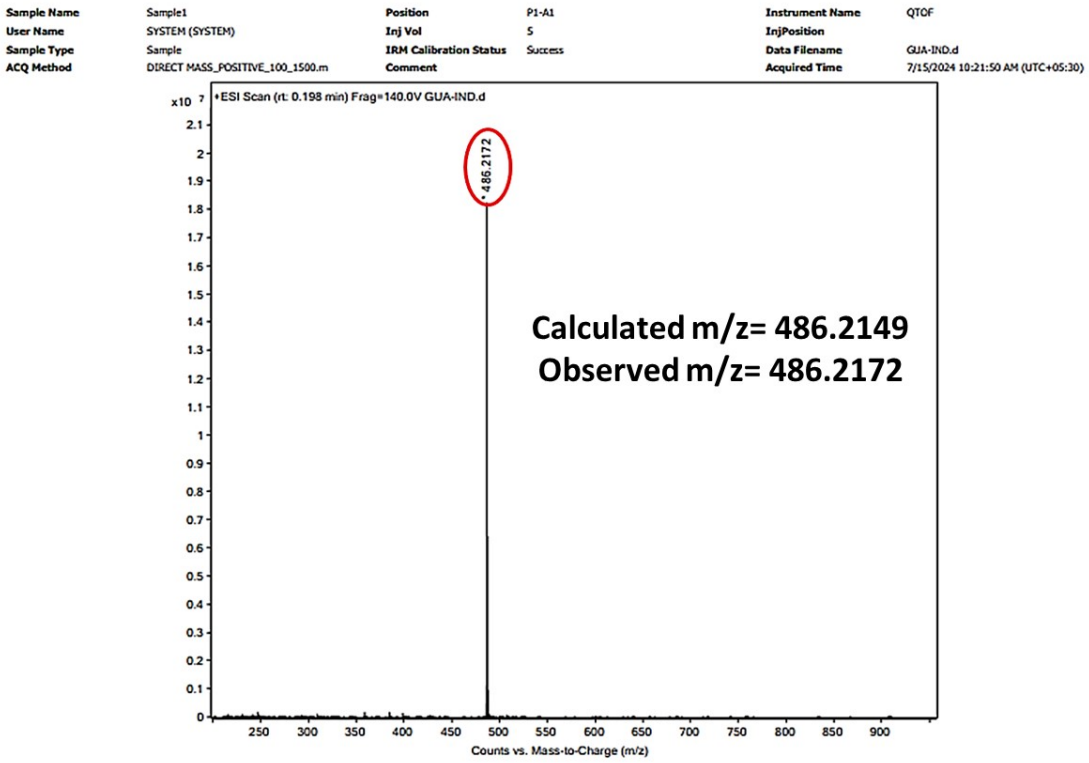

Figure S3. HRMS of **GUA-IND**.

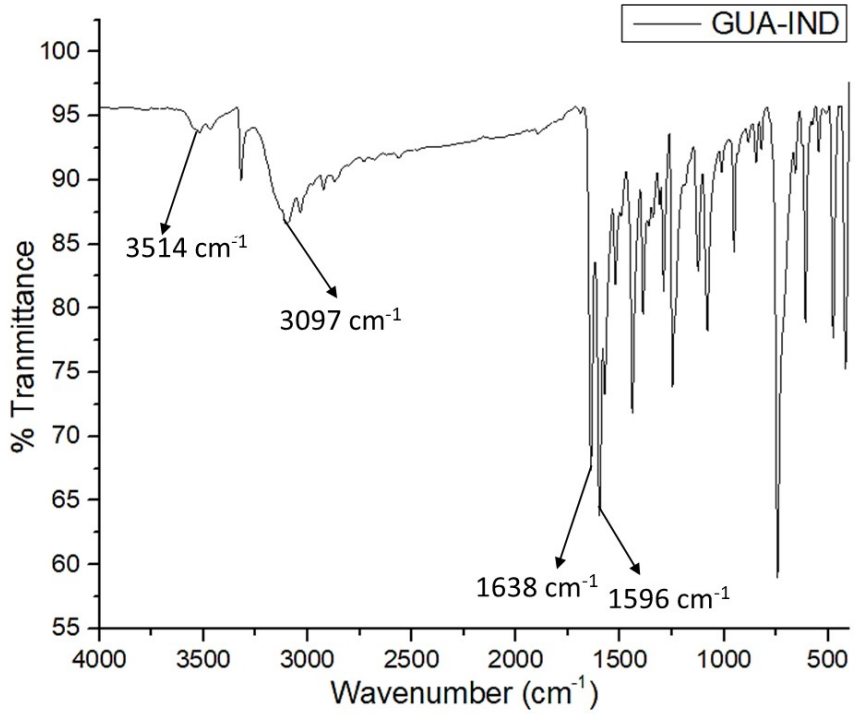

Figure S4. FT-IR spectrum of **GUA-IND**.

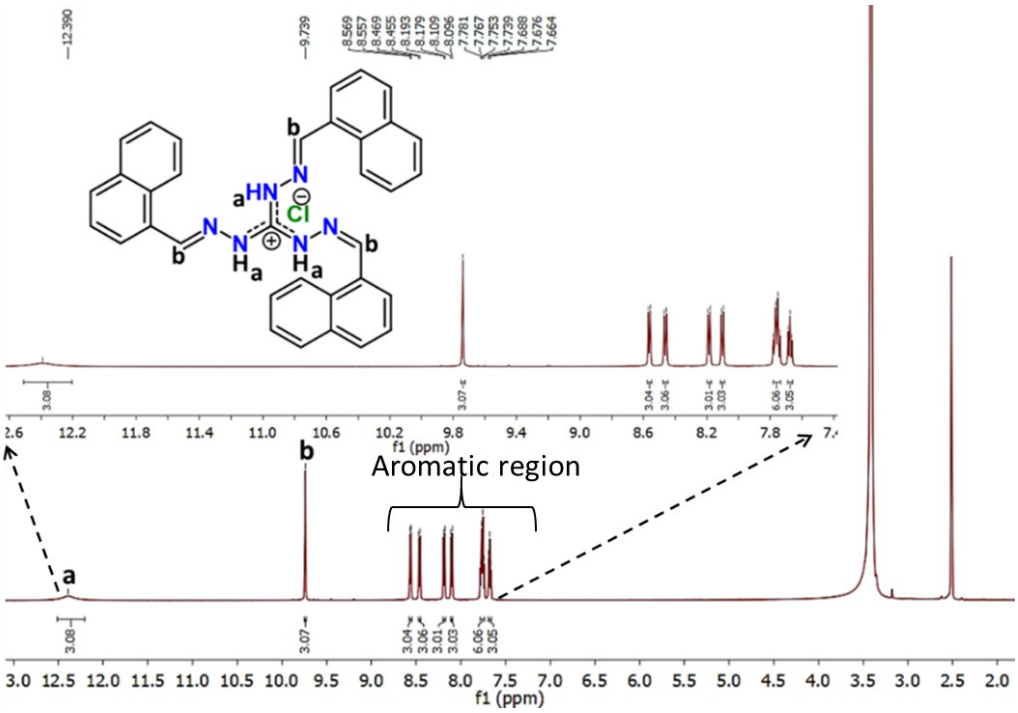

Figure S5. ^{1}H NMR spectrum of **GUA-NAP** in DMSO-d_6.

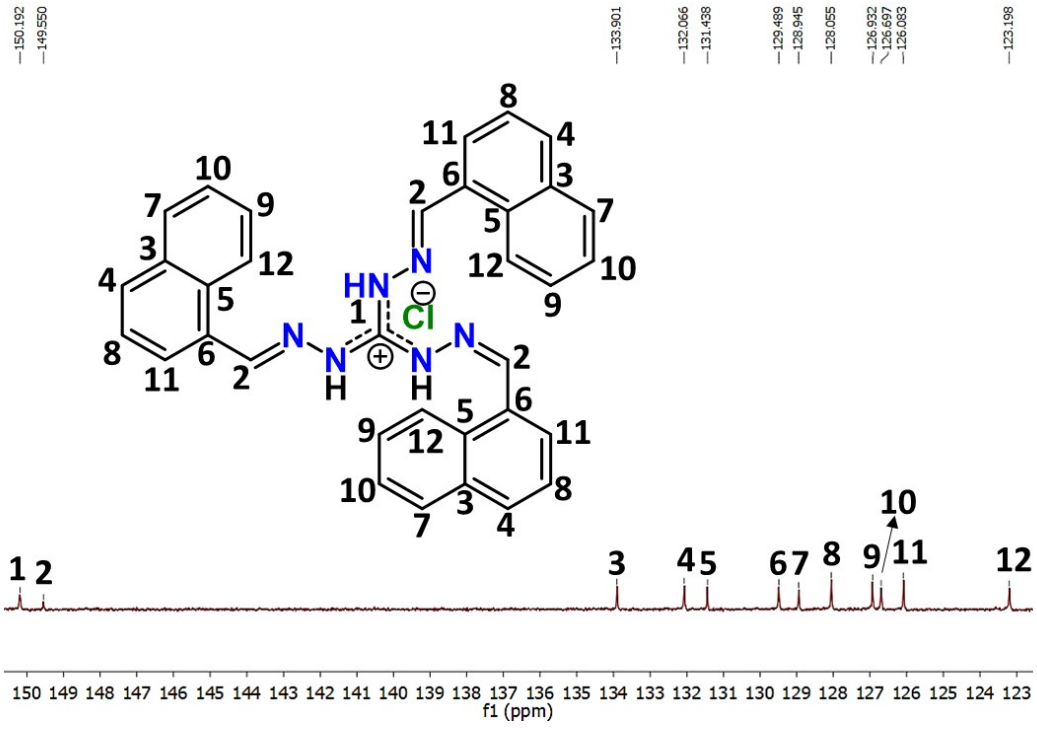

Figure S6. ^{13}C NMR spectrum of **GUA-NAP** in DMSO-d_6.

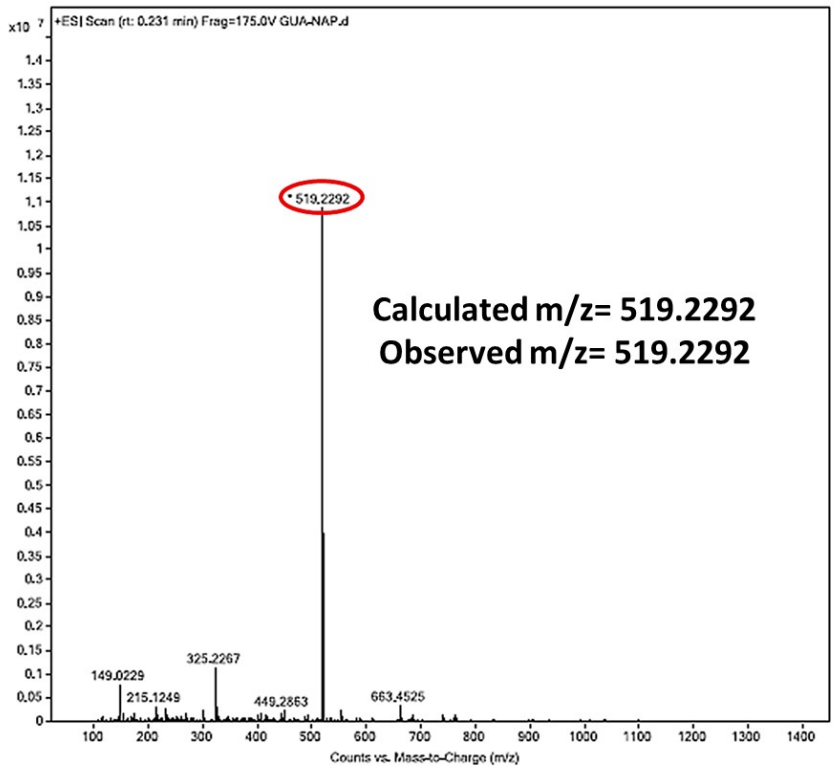

Figure S7. HRMS of **GUA-NAP**

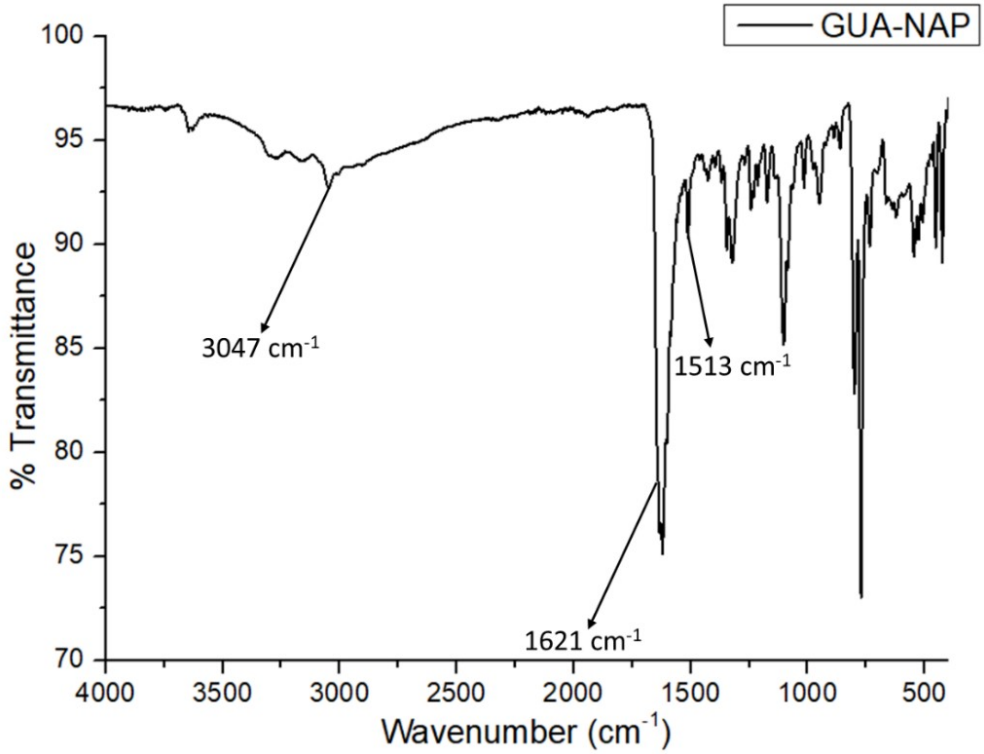

Figure S8. FT-IR spectrum of **GUA-NAP**.

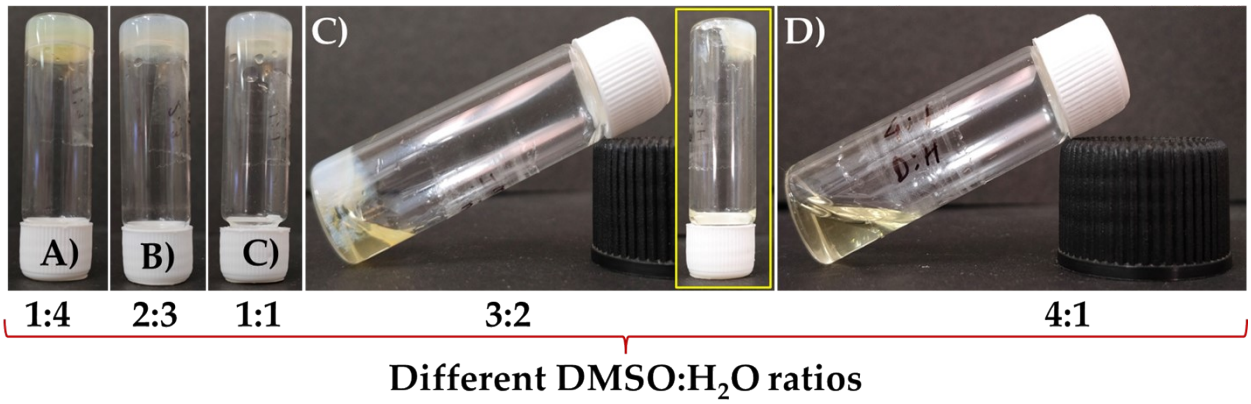

Figure S9. Gelation studies of **GUA-IND** with $(TBA)_2SO_4$ in different ratios of DMSO: H_2O viz. A) 1:4, B) 2:3, C) 1:1, D) 3:2 and E) 4:1.

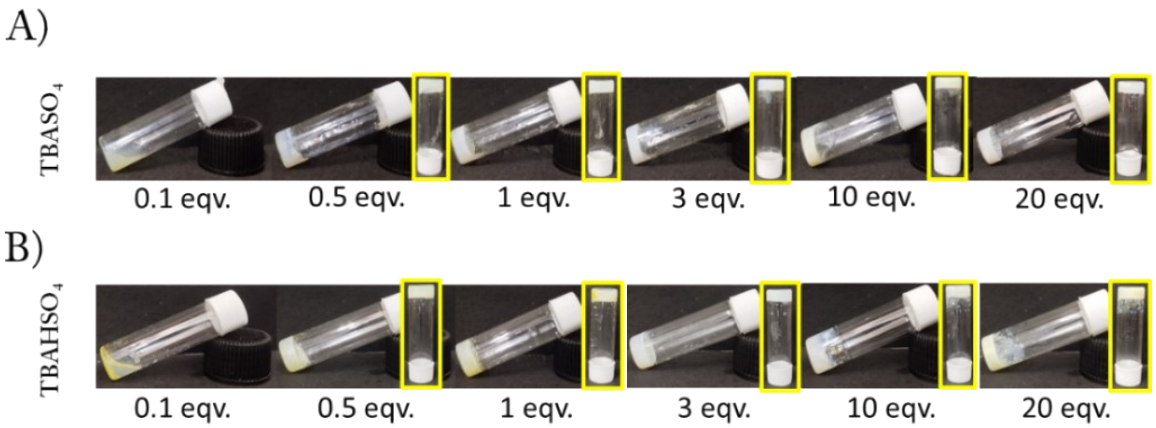

Figure S10. Different concentration of A) $(TBA)_2SO_4$ and B) $TBAHSO_4$ used for formation of gel with **GUA-IND**.

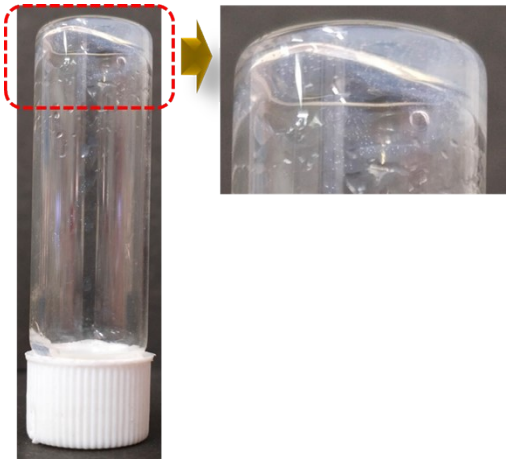

Figure S11. The minimum gelation concentration of **GUA-IND** required for gelation with $(TBA)_2SO_4$.

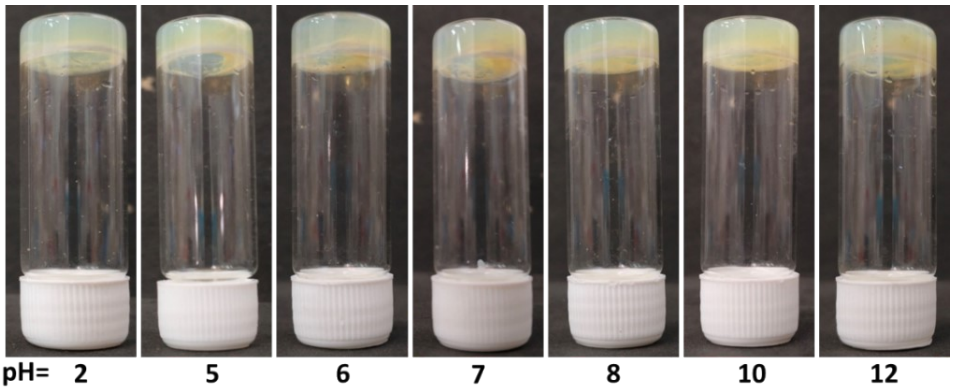

Figure S12. GI-G gel formation at different pH.

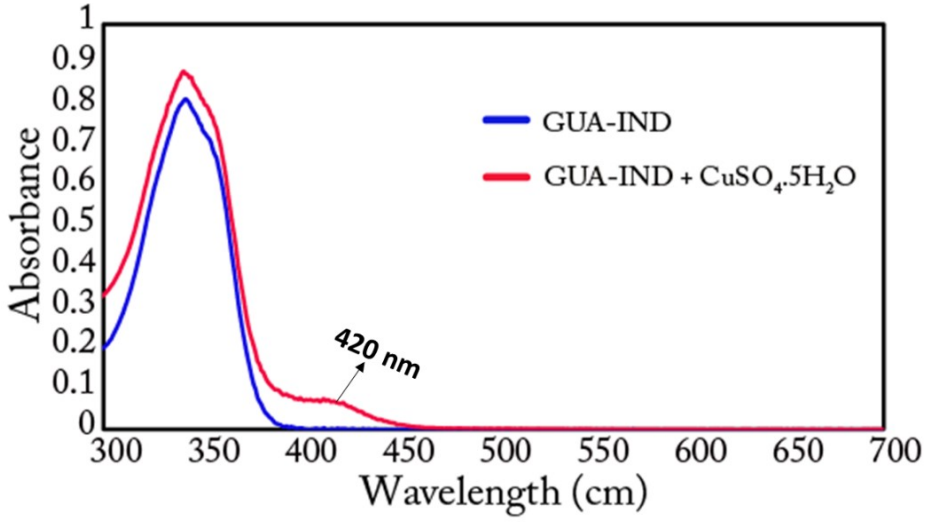

Figure S13. Absorption spectra of **GUA-IND** in presence and absence of $CuSO_4.5H_2O$.

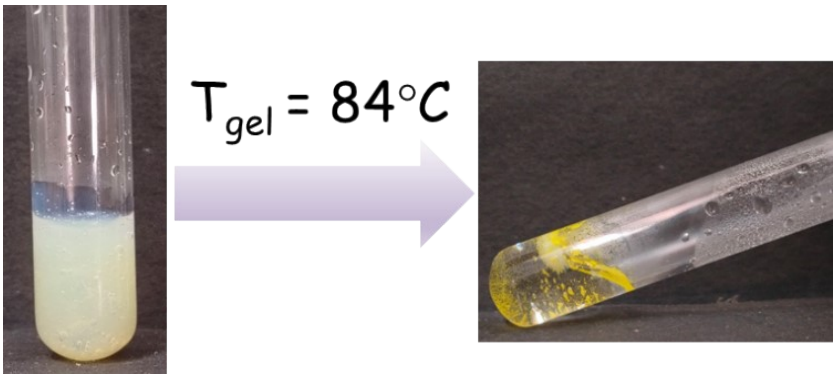

Figure S14. Gel-to-sol transition of **GI-G** gel.

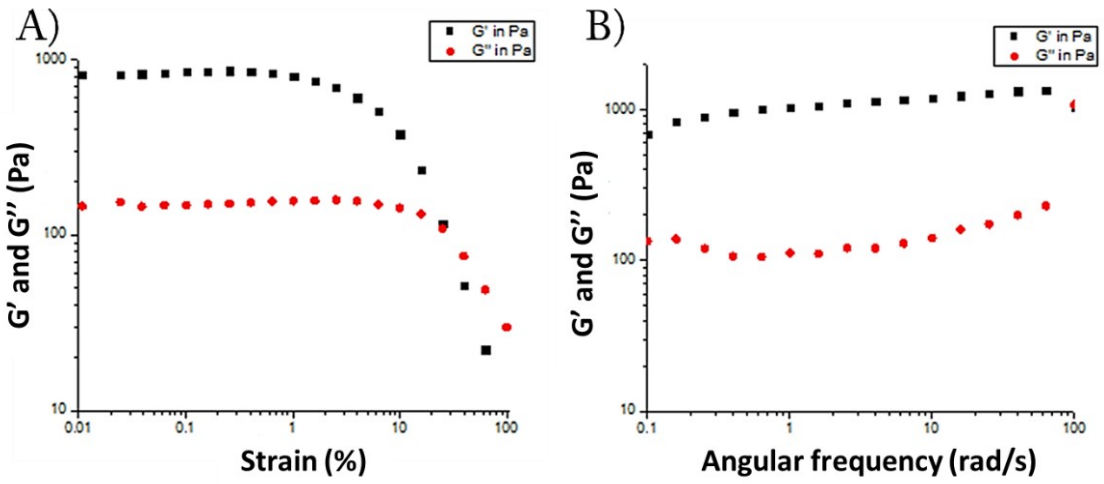

Figure S15. A) Amplitude sweep and B) frequency sweep of the **GI-G** gel.

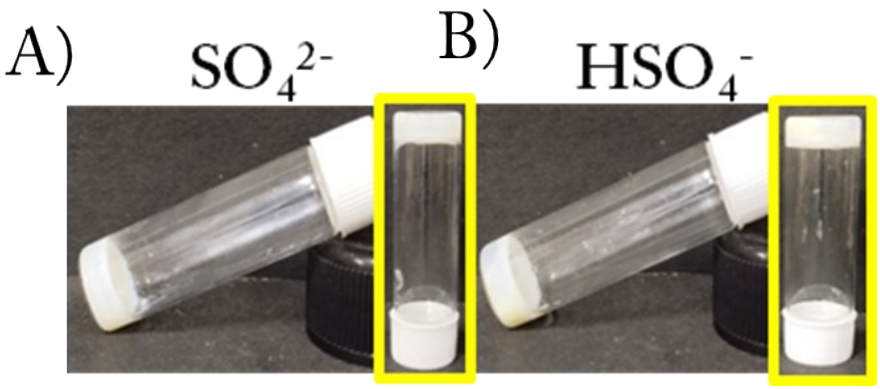

Figure S16. Gelation study of **GUA-IND** in DMF: H_2O (1:4, v/v) in the presence of A) SO_4^{2-} and B) HSO_4^-.

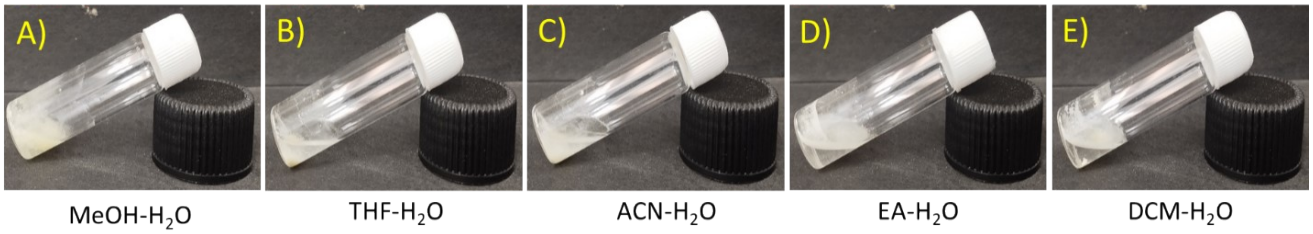

Figure S17. Gelation study of **GUA-IND** with SO_4^{2-} in A) MeOH (methanol)-H_2O, B) THF (tetrahydrofuran)-H_2O, C) ACN (acetonitrile)-H_2O, D) DCM (dichrolomethane)-H_2O D) EA (ethylacetate)-H_2O.

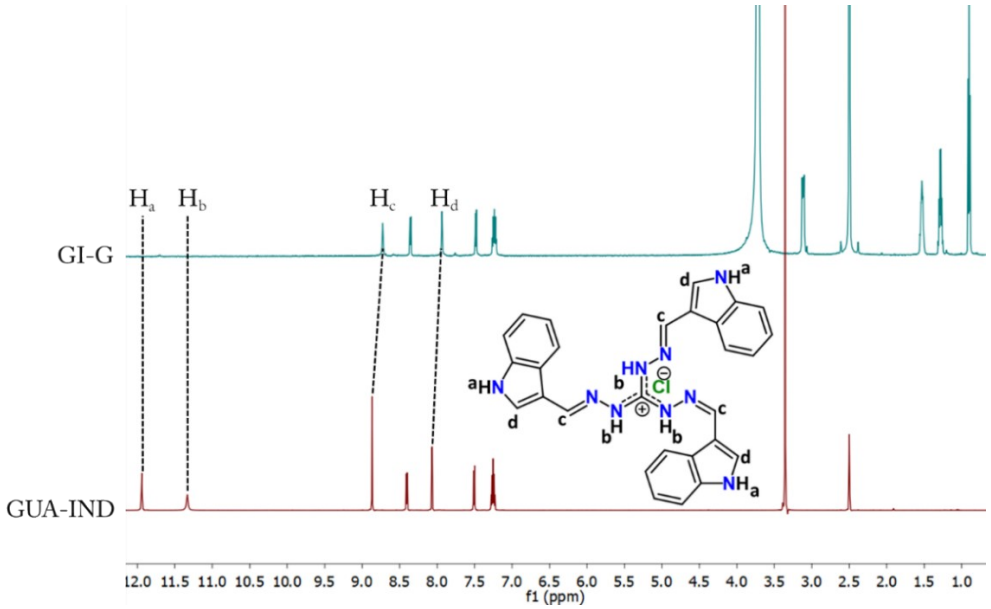

Figure S18. Stacked ^{1}H NMR spectra of **GUA-IND** and **GI-G**.

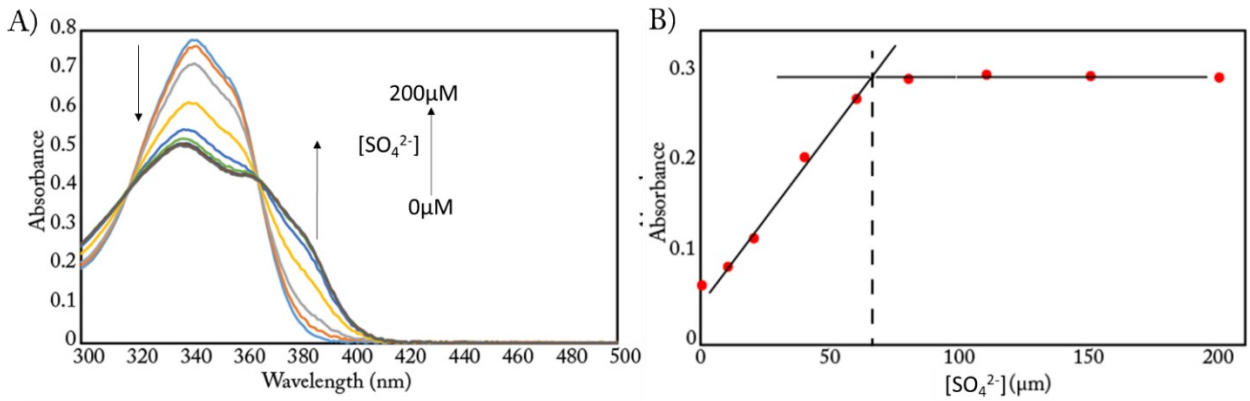

Figure S19. A) UV-Vis spectra of **GUA-IND** with increasing concentration of SO_4^{2-} anion, B) plot of absorbance vs. $[SO_4^{2-}]$ anion at 385 nm wavelength.

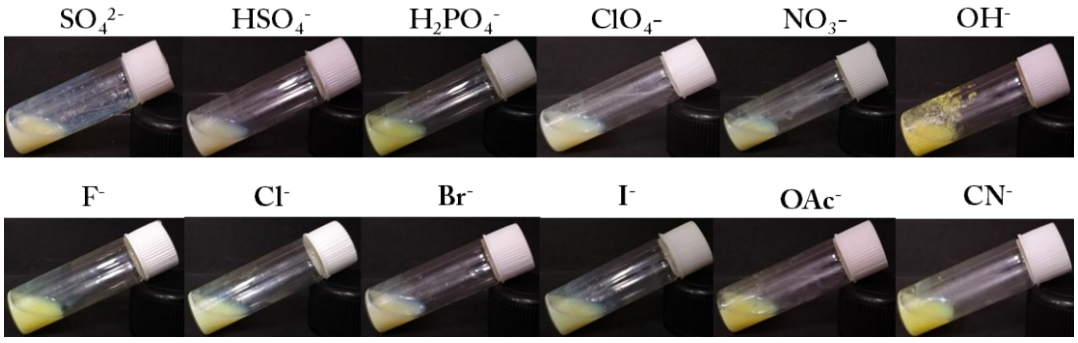

Figure S20. Gelation study of **GUA-NAP** in DMSO-H_2O (1: 4, v/v) in the presence of different anions of TBA salts.

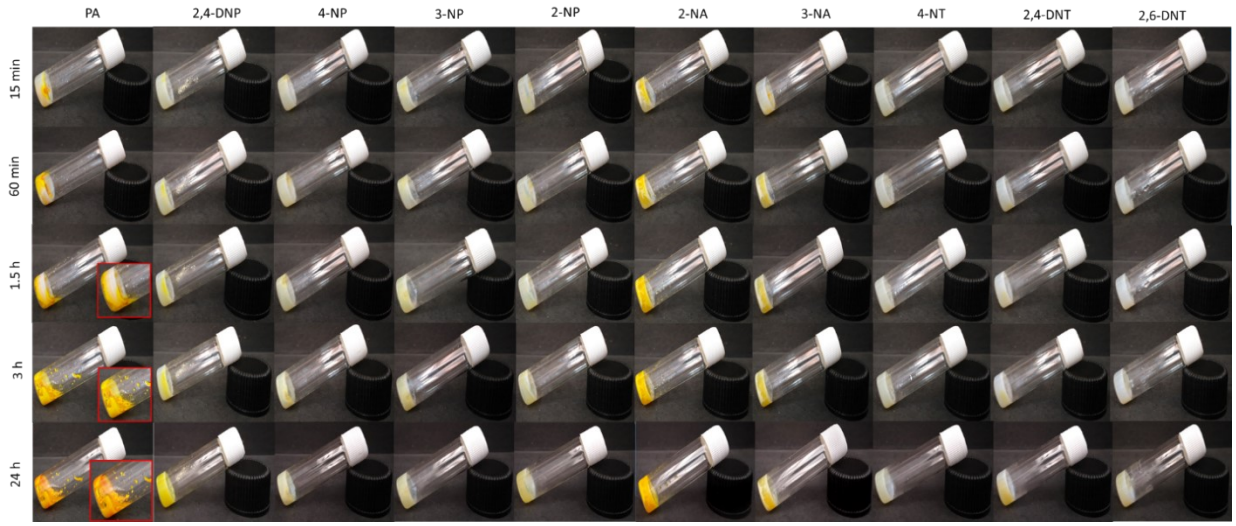

Figure S21. Stimuli responsive behaviour of **GUA-IND** towards different nitro-aromatic compounds at different time-intervals.

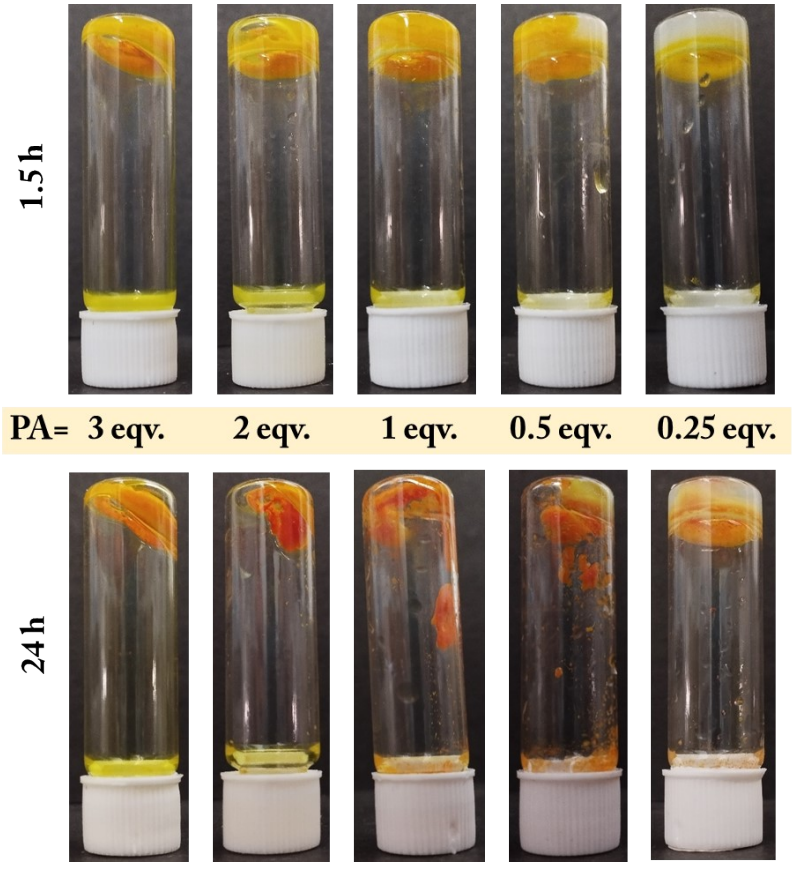

Figure S22. GI-G gel after addition of different equivalents of PA**.**

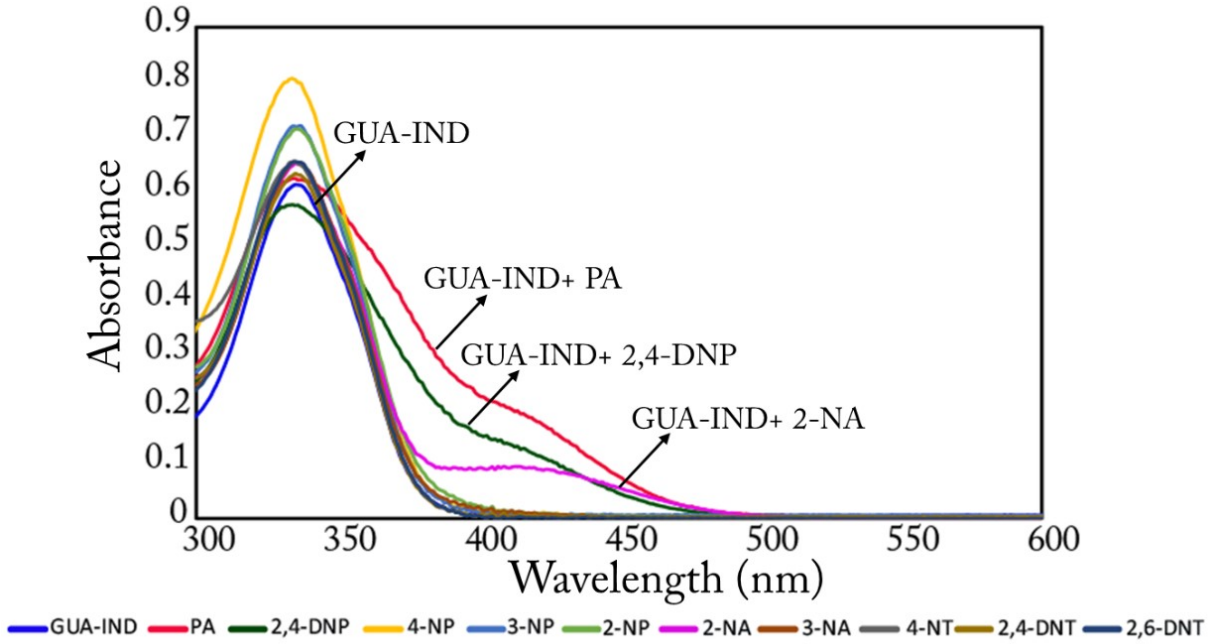

Figure S23. UV-Vis spectra of **GUA-IND** in presence of different nitro-aromatic compounds in H_2O.

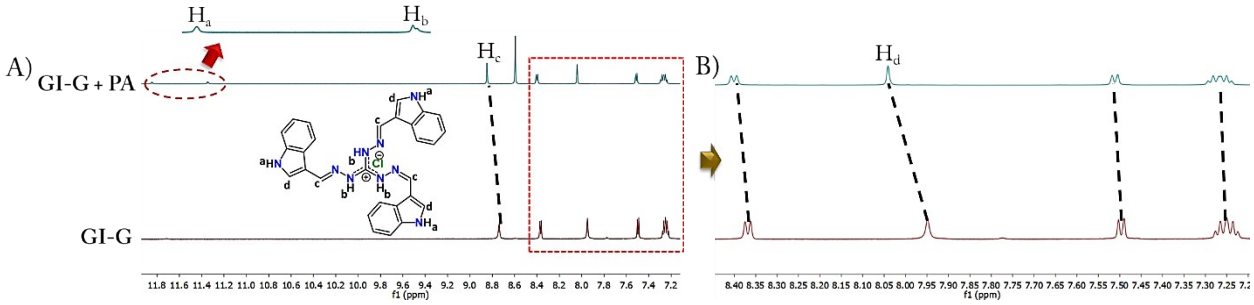

Figure S24. ^{1}H NMR spectra of A) **GI-G** and B) **GI-G** + PA in DMSO-*d6*.

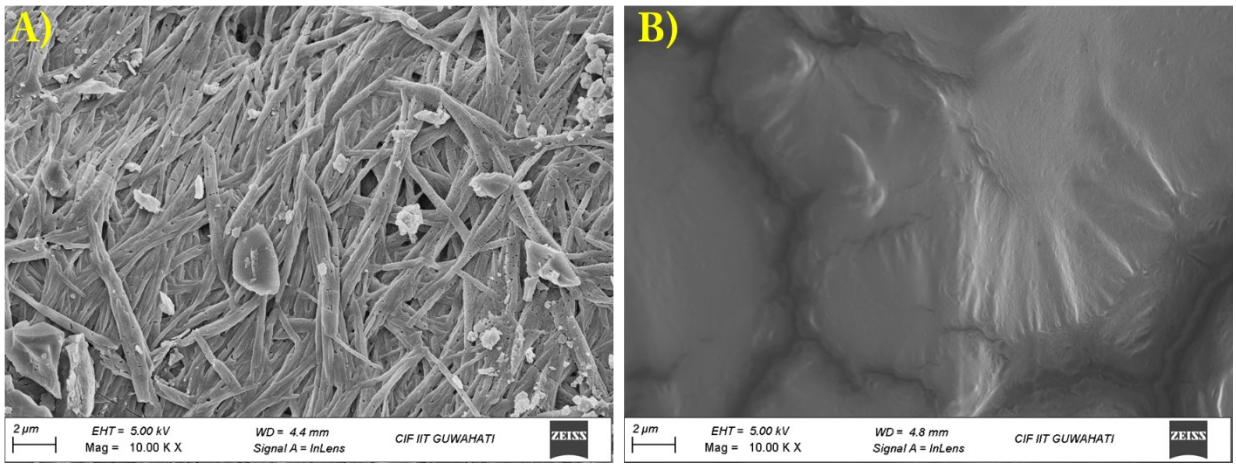

Figure S25. FESEM images of A) **GI-G** xerogel and B) **GI-G** + PA xerogel

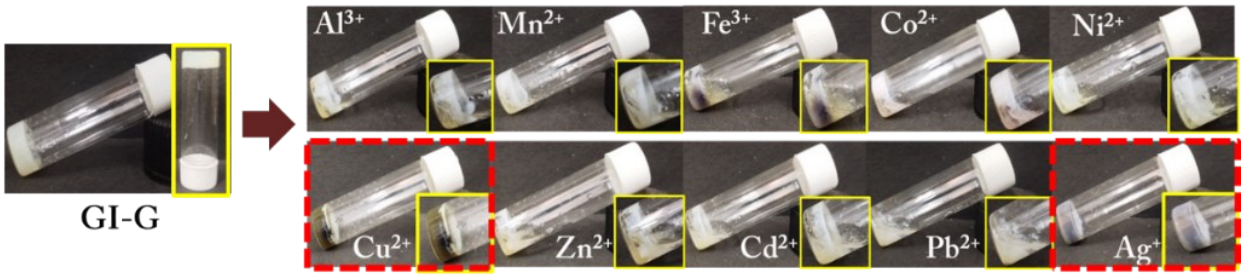

Figure S26. Effect of different metal salts on **GI-G** gel.

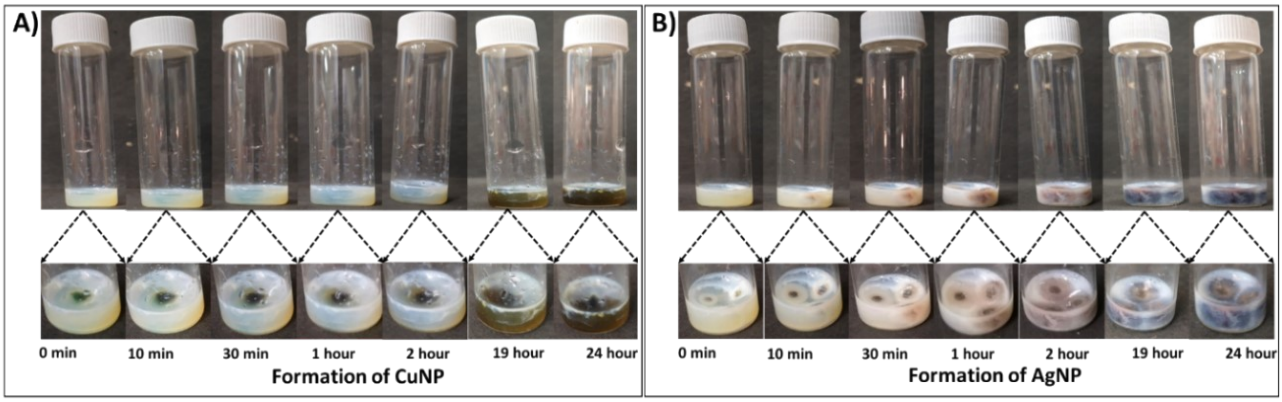

Figure S27. Formation of A) CuNPs and B) AgNPs.

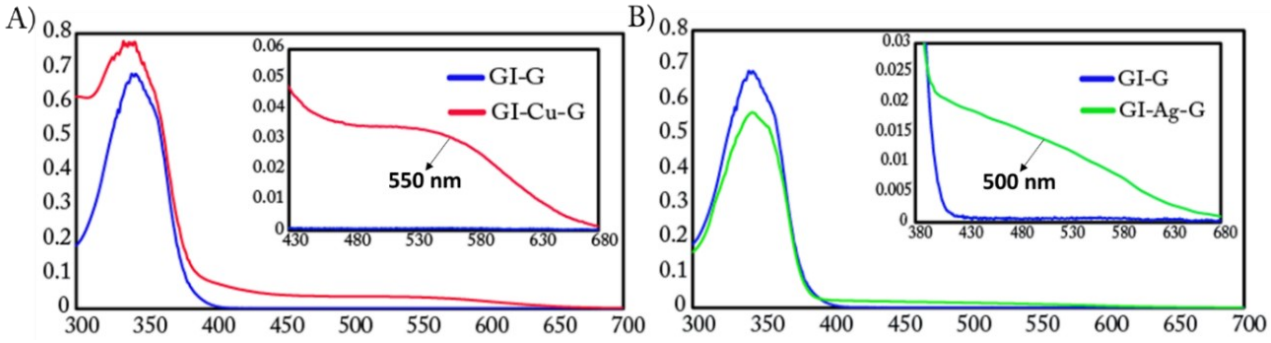

Figure S28. UV-Vis spectra of A) **GI-Cu-G** and B) **GI-Ag-G** gel nanocomposites dissolved in DMSO.

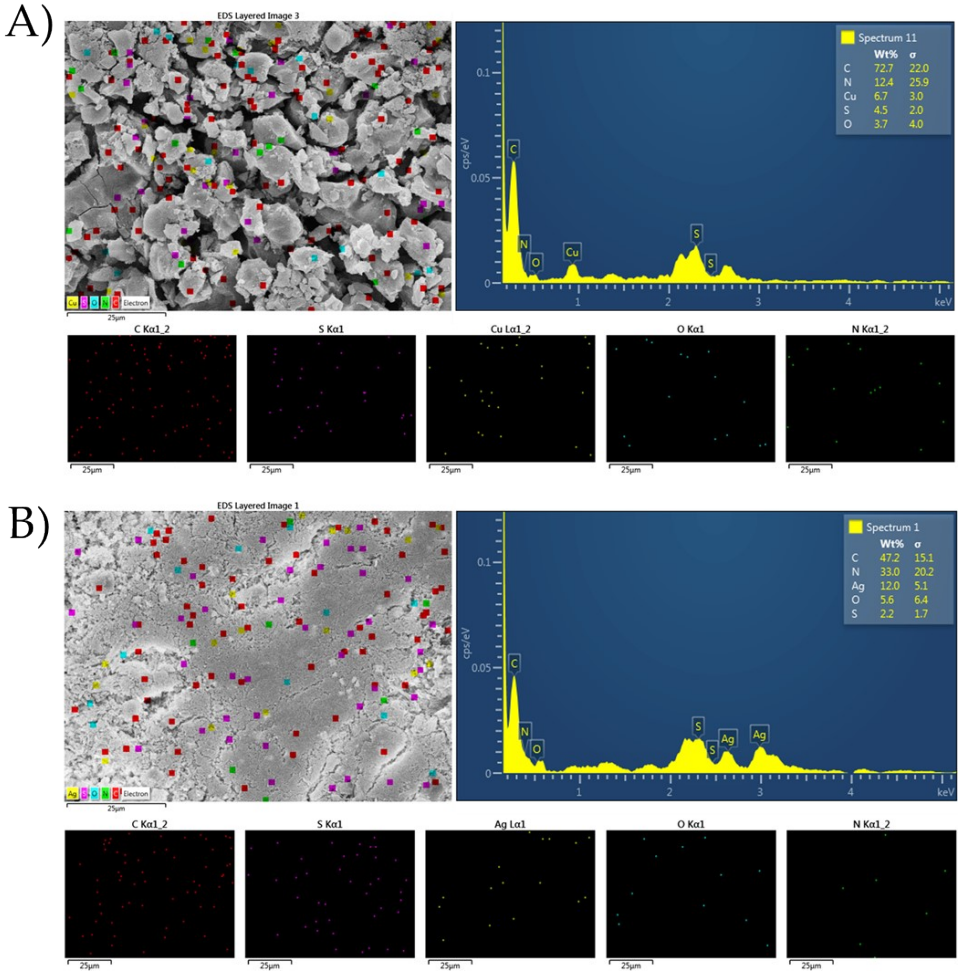

Figure S29. Energy dispersive X-ray (EDX) spectrum analysis of A) **GI-Cu-G** and B) **GI-Ag-G** xerogel. C: carbon, N: nitrogen; S: sulphur; O: oxygen; Cu: copper, Ag: silver.

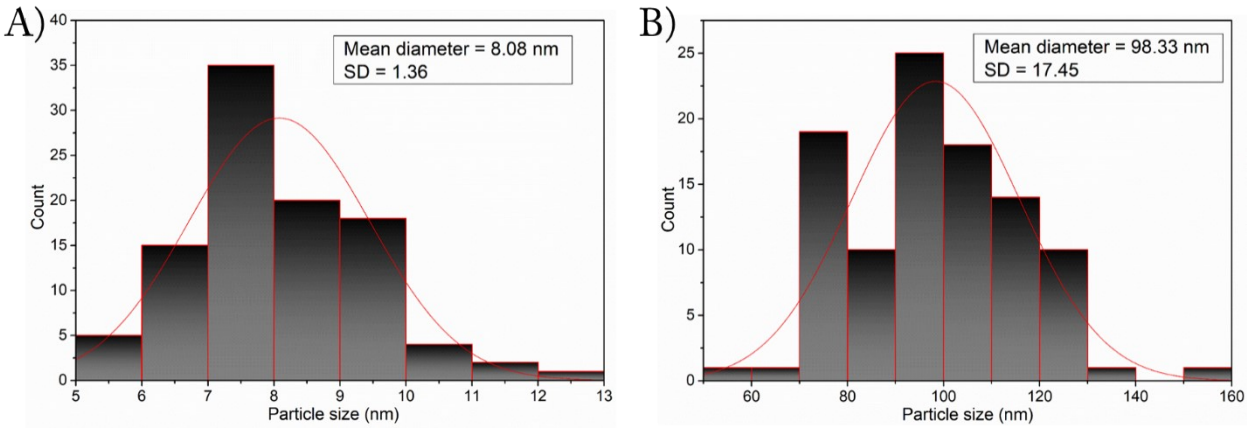

Figure S30. Histogram of the particle size distribution of A) **GI-Cu-G** and A) **GI-Ag-G**.

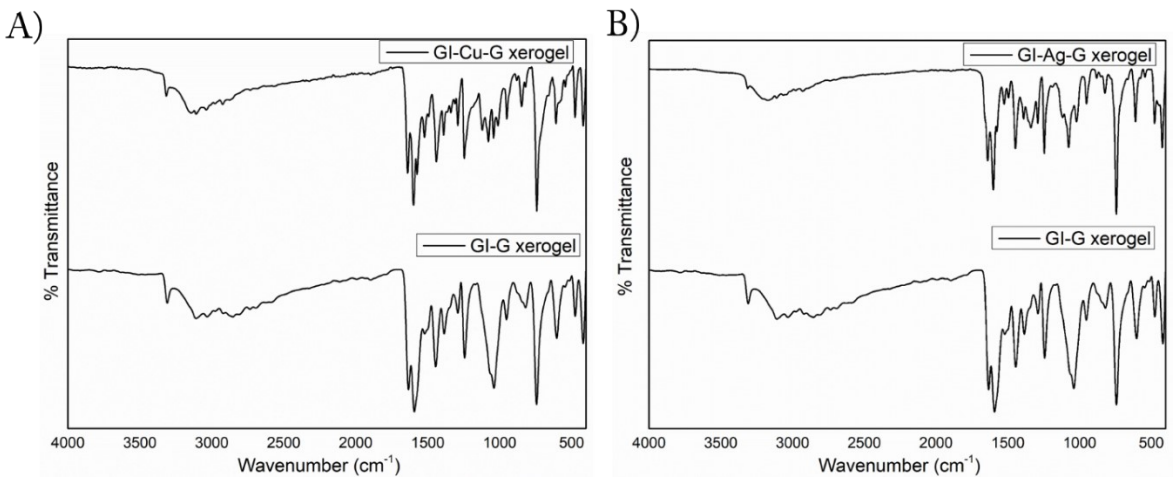

Figure S31. Stacked IR spectra of A) **GI-Cu-G** and **GI-G** and B) **GI-Ag-G** and **GI-G** xerogel in DMSO-d_6.

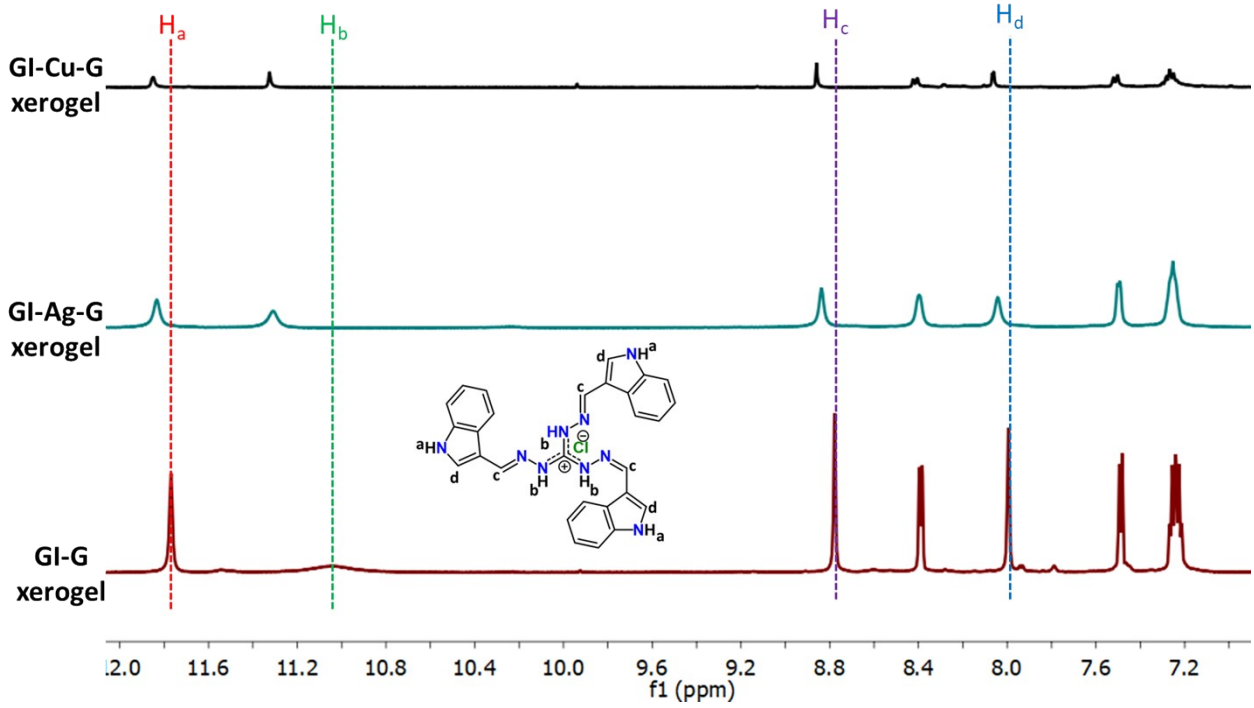

Figure S32. Stacked ^{1}H NMR spectra of **GI- G**, **GI-Cu-G** and **GI-Ag-G** xerogel in DMSO-d_6.

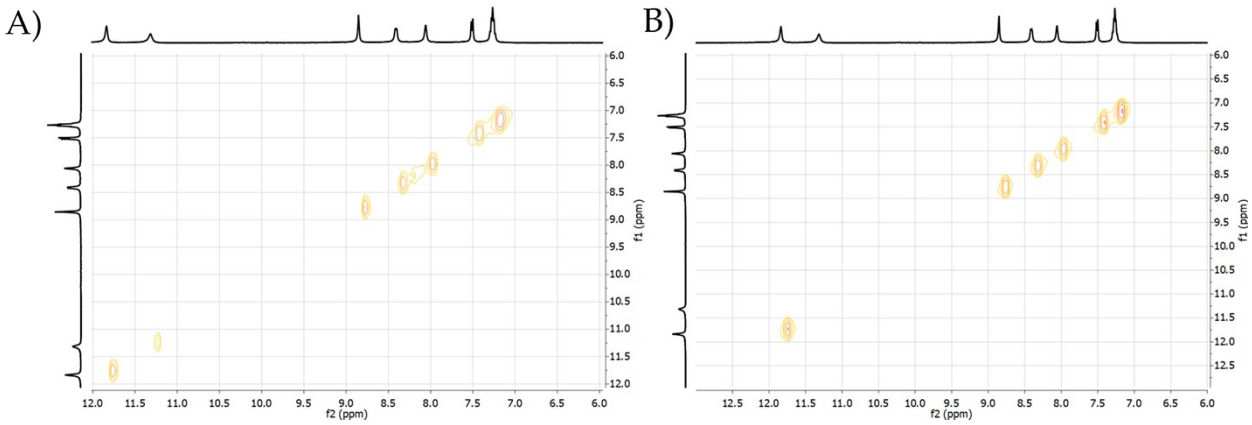

Figure S33. NOESY spectra of A) **GI-Cu-G** and B) **GI-Ag-G** xerogel in DMSO-d_6.

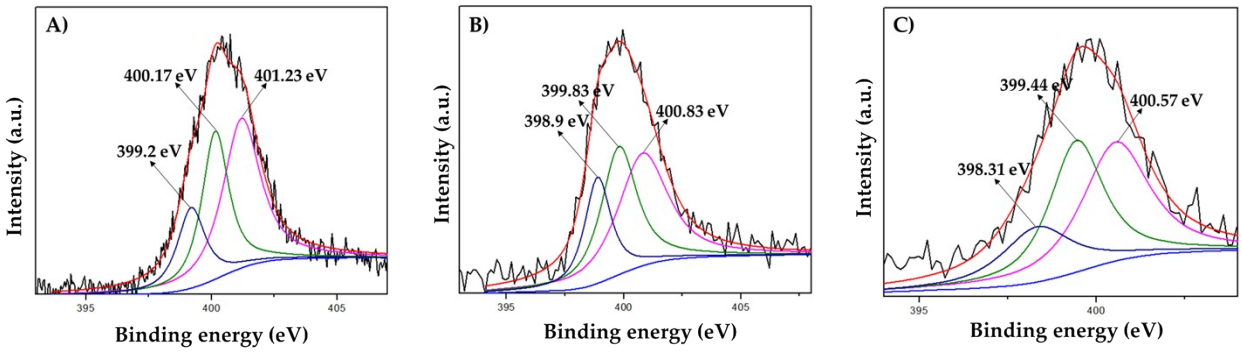

Figure S34. XPS spectra of N1s of A) **GI- G,** B) **GI-Cu-G** and A) **GI-Ag-G** xerogel.

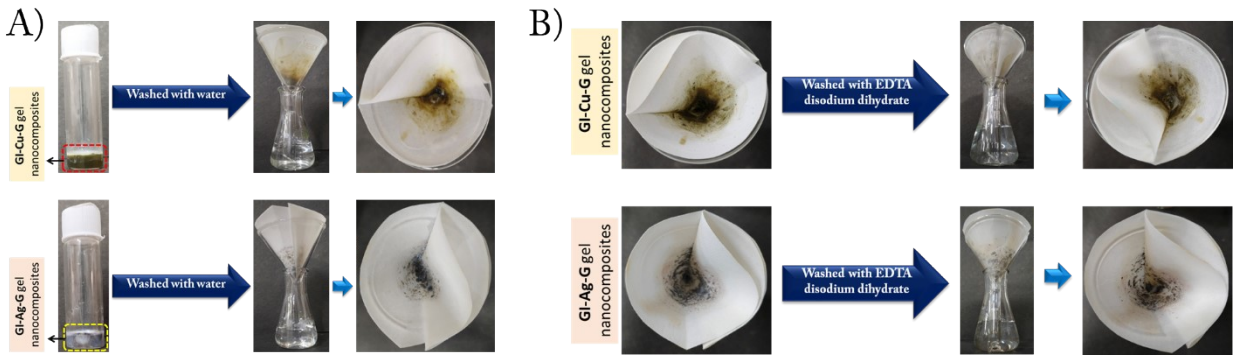

Figure S35. Images of **GI-Cu-G** and **GI-Ag-G** gels A) washed with water B) washed with EDTA disodium dihydrate.

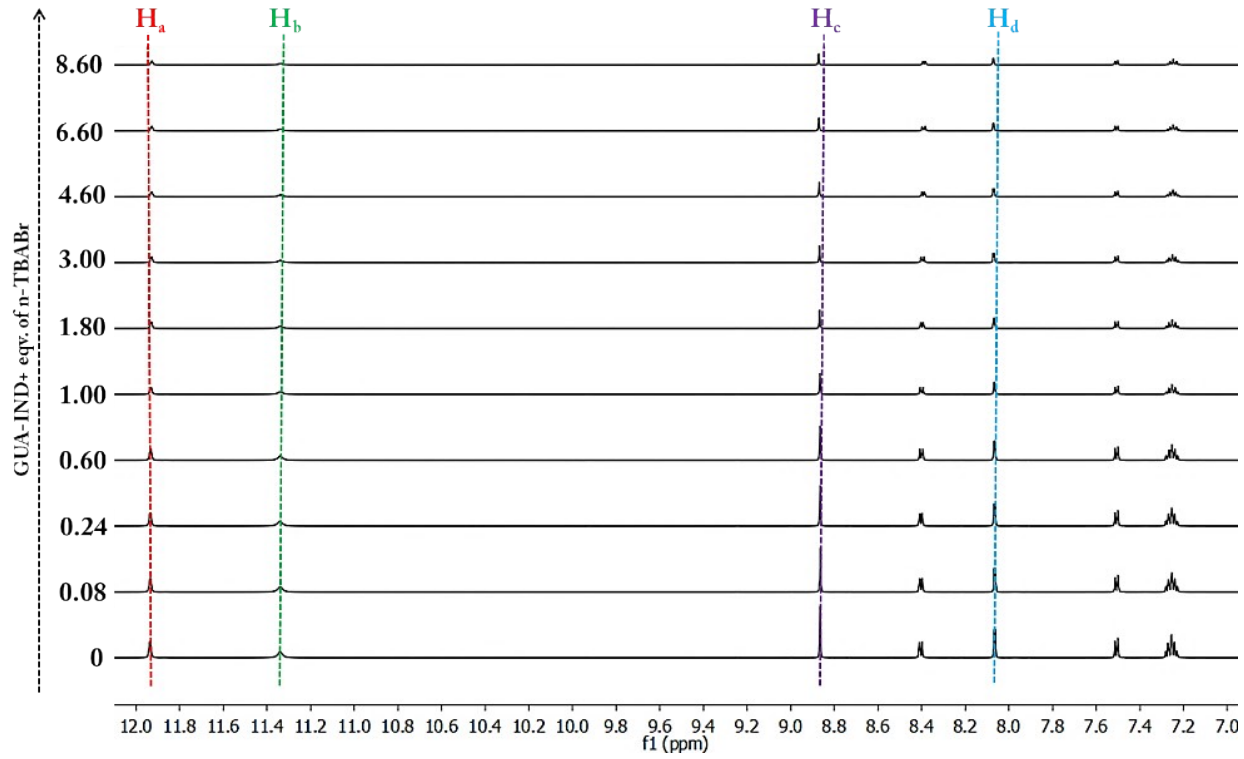

Figure S36. ^{1}H NMR titration of **GUA-IND** in DMSO-d_6 with increasing concentration of Br^-.

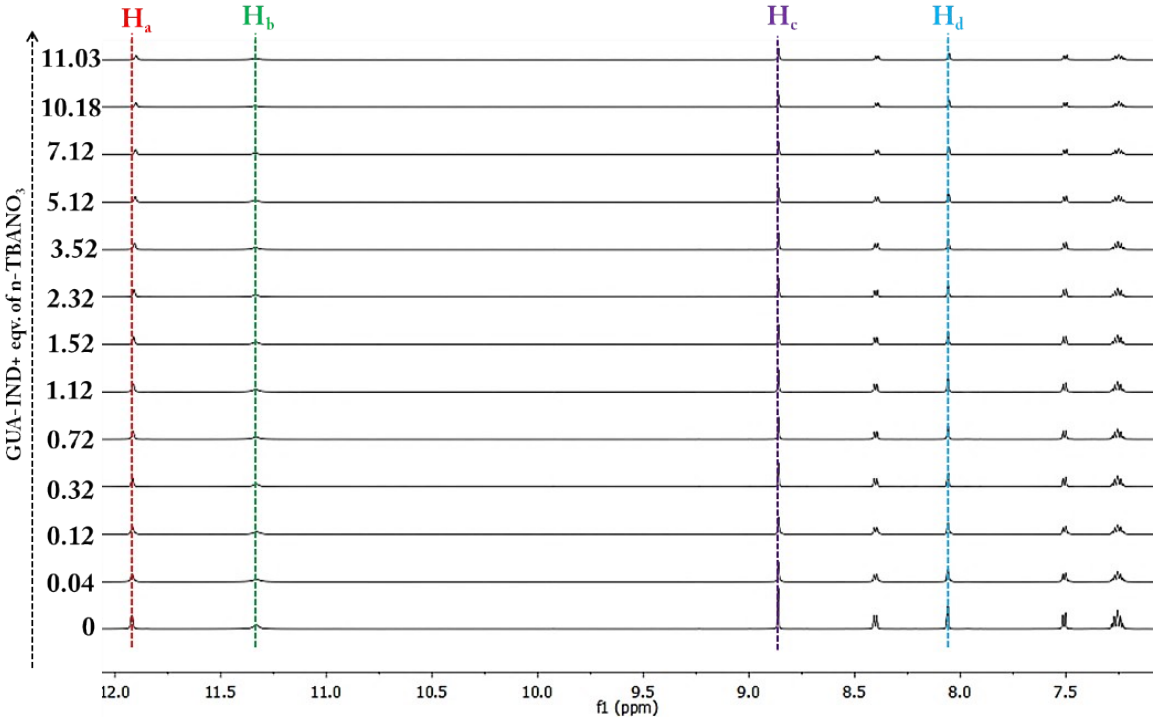

Figure S37. ^{1}H NMR titration of **GUA-IND** in DMSO-d_6 with increasing concentration of NO_3^-.

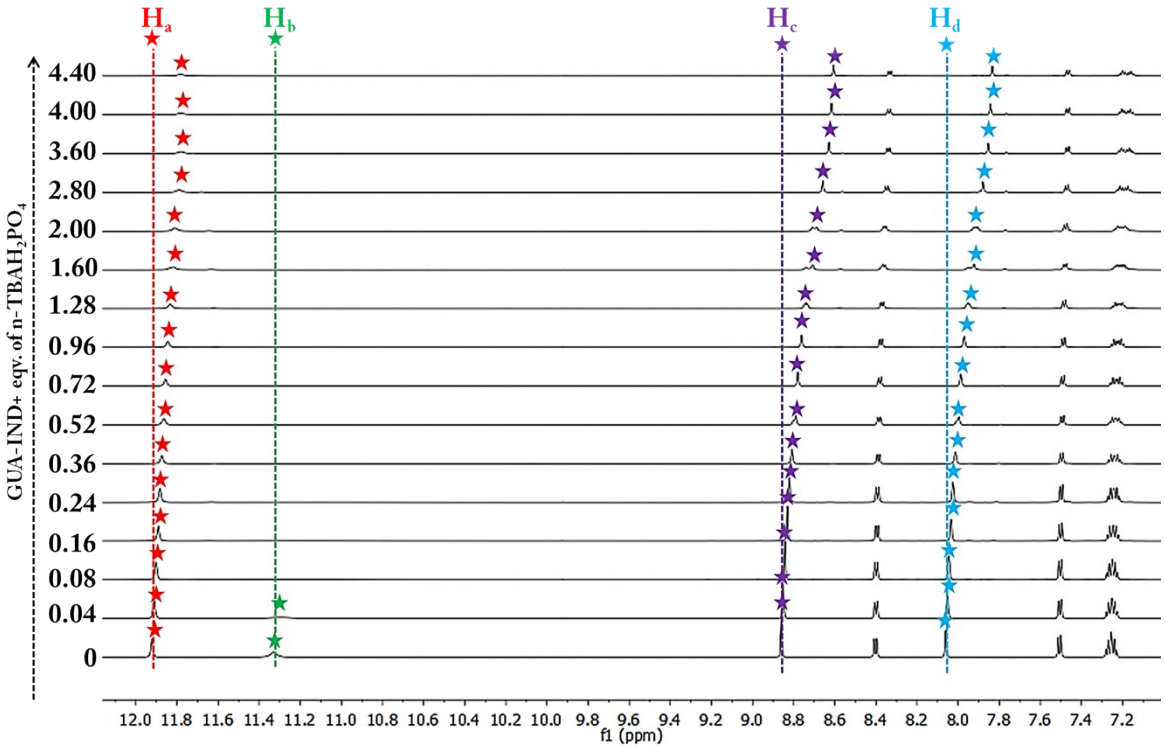

Figure S38. ^{1}H NMR titration of **GUA-IND** in DMSO-d_6 with increasing concentration of $H_2PO_4^-$.

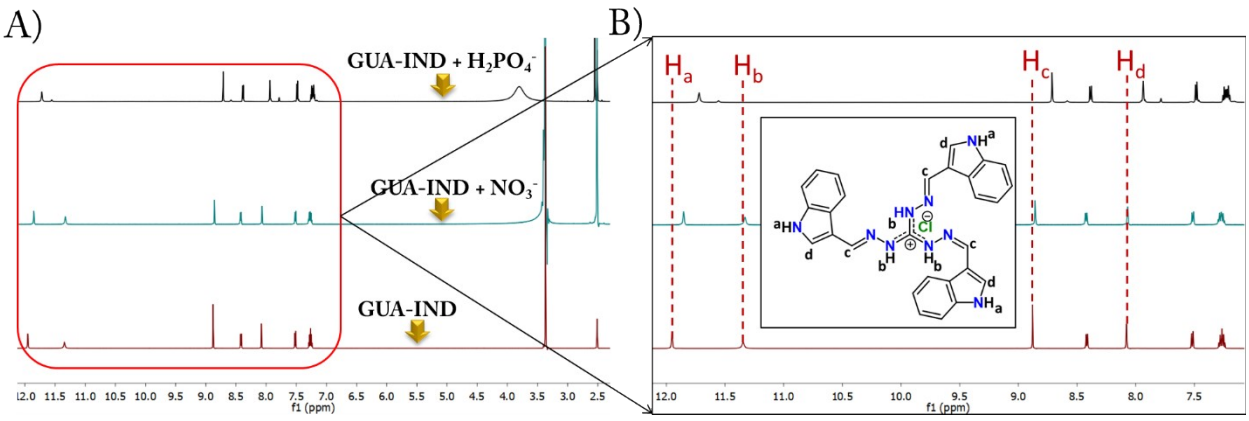

Figure S39. Stacked ^{1}H NMR spectra of **GUA-IND**, **GUA-IND** + NO_3^-, **GUA-IND** + $H_2PO_4^-$ in DMSO-d_6.

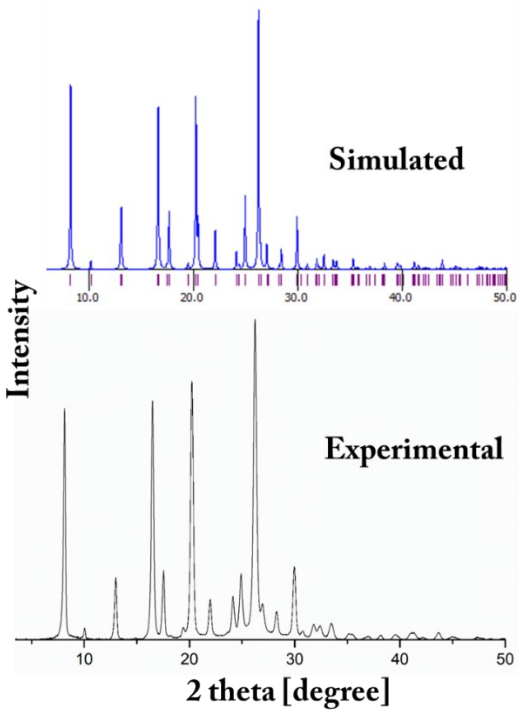

Figure S40. Powder X-ray diffraction: simulated pattern from the single-crystal X-ray of **[GUA-IND.NO_3]$^-$** (blue), experimental pattern from the crystalline solid of **[GUA-IND.NO_3]$^-$** (black).

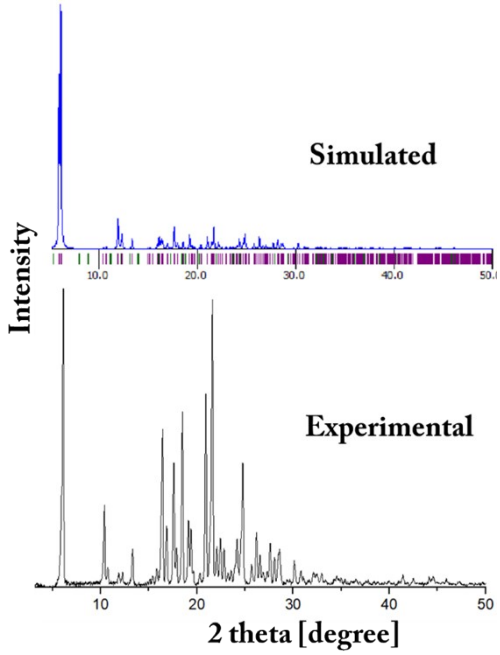

Figure S41. Powder X-ray diffraction: simulated pattern from the single-crystal X-ray of **[GUA-IND.H_2PO_4]$^-$** (blue), experimental pattern from the crystalline solid of **[GUA-IND. H_2PO_4] $^-$** (black).

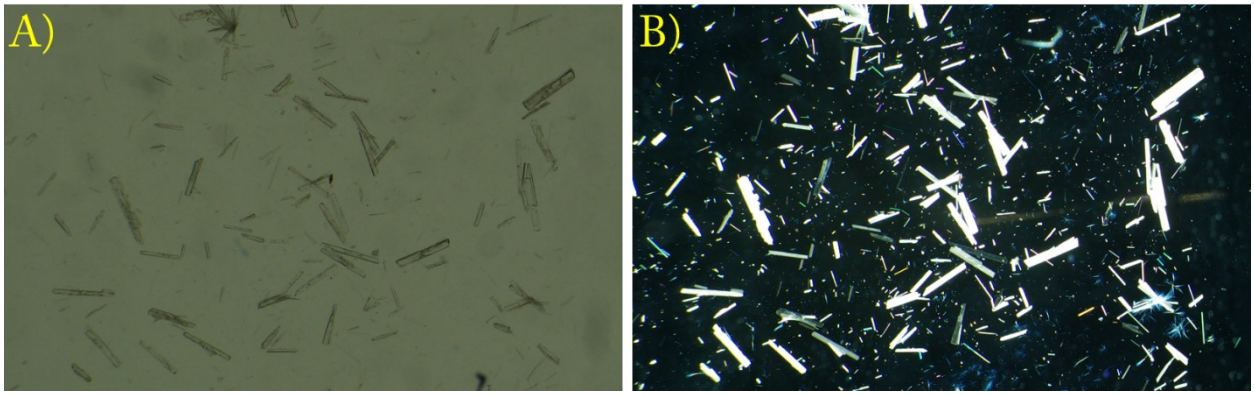

Figure S42. A) Bright field and B) Polarised microscopic image of **[GUA-IND.H_2PO_4]$^-$** crystals.

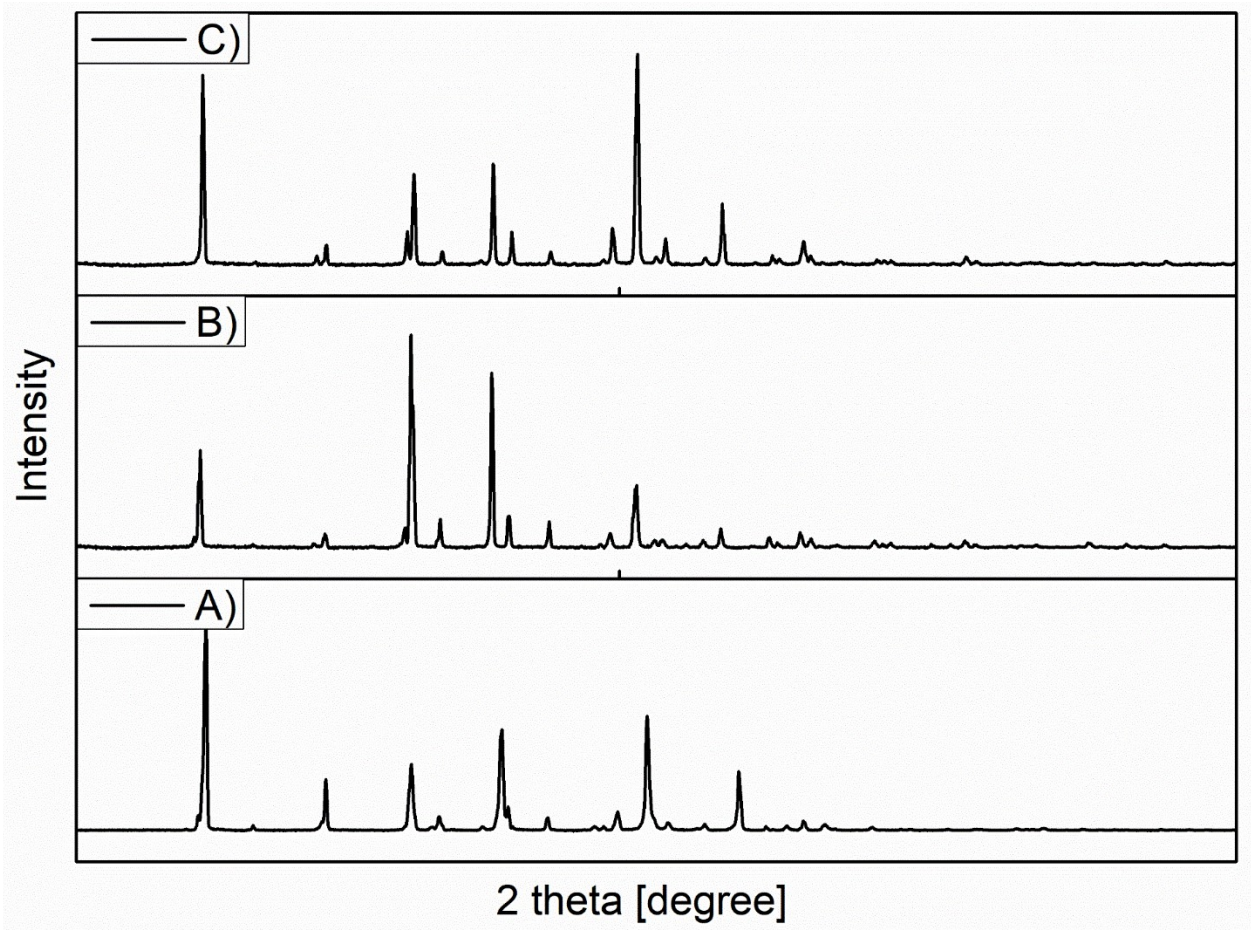

Figure S43. Stacked PXRD spectra of A) crystals of **GUA-IND** obtained from crystallisation of **GUA-IND** in DMSO, B) crystals of **GUA-IND** obtained after reversible anion exchange of Cl^- with **[GUA-IND.NO_3]$^-$** and C) crystals of **GUA-IND** obtained after reversible anion exchange of Cl^- with **[GUA-IND. H_2PO_4]$^-$**.

Table S1. Crystallographic parameters and refinement data of the receptors and anionic complex

Parameters	Gua-IND	$[GUA\text{-}IND.Br]^-$	$[GUA\text{-}IND.NO_3]^-$	$[GUA\text{-}IND.H_2PO_4]^-$
formula	$C_{56}\ H_{48}\ Cl\ N_{18}$	$C_{28}\ H_{24}\ Br\ N_9$	$C_{28}\ H_{24}\ N_{10}\ O_3$	$C_{30}\ H_{32}\ N_9\ O_5\ P\ S$
fw	1008.57	566.47	548.57	661.67
cryst syst	trigonal	trigonal	trigonal	orthorhombic
space group	R -3 :H	R -3 :H	R -3 :H	P n a 21
a (Å)	16.4700(6)	17.310(2)	17.333(3)	8.2595(4)
b (Å)	16.4700(6)	17.310(2)	17.333(3)	16.3723(8)
c (Å)	15.5495(8)	15.538(4)	15.209(3)	29.5080(14)
α (deg)	90	90	90	90
β (deg)	90	90	90	90
γ (deg)	120	120	120	90
V ($Å^3$)	3652.9(3)	4031.8(15)	3957.1(15)	3990.3(3)
Z	3	6	6	4
DC ($g\ cm^{-3}$)	1.375	1.400	1.381	1.101
μ (Mo Kα) (mm^{-1})	0.140	1.565	0.096	0.165
F (000)	1581.0	1740.0	1716.0	1384.0
T (K)	298 K	295 K	297 K	295 K
θmax (deg)	24.973	24.984	26.406	26.379
total no. of rflns	27090	32366	33633	61785
no. of indep rflns	1396	1577	1800	8088
no. of obsd rflns	1250	1362	1354	4958
no.of params refined	114	115	132	419
R1, I > 2σ(I)	0.1393(1250)	0.0872(1362)	0.0529(1354)	0.0923(4958)
wR2, I > 2σ(I)	0.4276(1396)	0.2595(1577)	0.1762(1800)	0.1907(8088)
GOF (F^2)	2.177	1.096	1.056	1.059
CCDC no.	2419337	2419425	2419339	2419341

of **GUA-IND**.

Table S2. Hydrogen bonding distances (Å) and Bond angles (º) in the neutral receptors and their anionic complexes.

Ligand/Complex	D H···A	d(D···H)/Å	d(H···A)/Å	d(D···A)/Å	<D-H···A/	Symmetry codes
GUA-IND	N3-H3N···N2	0.86	2.36	2.665 (5)	101	-x+y, 1-x, z
[GUA-IND.Br]$^-$	N1-H1N···Br1	0.86	2.45	3.264 (5)	158	x, y, z
	N3-H3N···N2	0.86	2.35	2.657 (7)	102	-x+y, 1-x, z
[GUA-IND.NO_3]$^-$	N1-H1N···O1	0.95 (3)	2.20 (3)	3.039 (3)	147 (3)	x, y, z
	N1-H1N···O1	0.95 (3)	2.08 (3)	2.957 (5)	154 (3)	-y, x-y, z
	N3-H3N···N2	0.88 (3)	2.30 (3)	2.655 (3)	104.2 (19)	-x+y, 1-x, z
[GUA-IND.H_2PO_4]$^-$	N1-H1···O3	0.86	2.03	2.860 (10)	162	1/2-x, -1/2+y, 1/2+z
	O1-H1B···O2	0.82	1.65	2.450 (9)	166	1/2+x,1/2- y, z
	N3-H3···N8	0.86	2.20	2.561 (9)	105	x, y, z
	N4-H4···O2	0.86	2.06	2.900 (11)	164	-1/2+x, 1/2-y, z
	O4-H4B···O3	0.82	1.70	2.516 (8)	171	-1/2+x, 1/2-y, z
	N6-H6···N2	0.86	2.38	2.696 (9)	102	x, y, z
	N6-H6···O5	0.86	2.56	3.194 (10)	132	-1/2+x, 1/2-y, z
	N7-H7A···O3	0.86	2.19	2.927 (11)	143	1/2-x, 1/2+y, ½+z
	N9-H9···O5	0.86	2.42	2.810 (9)	108	x, y, z

Table S3. Standard reduction potential of different metal ions.[9,10,11]

Half reaction	**Reduction potential (V)**
Al^{3+}/Al	-1.66
Mn^{2+}/Mn	-1.18
Zn^{2+}/Zn	-0.76
Cd^{2+}/Cd	-0.40
Ni^{2+}/Ni	-0.25
Pb^{2+}/Pb	-0.13
Cu^{2+}/Cu	+0.34
Ag^{+}/Ag	+0.80
Fe^{3+}/Fe^{2+}	+0.77

Co^{2+}/Co	−0.29

References

1. N. Zhang, X. Li, P. Li and S. Tang, *Int. J. Hydrogen Energy*., 2023, **48**, 25972-25983.

2. Apex 3; Bruker AXS Inc.: 2016.

3. Apex 4. Bruker AXS Inc.; 2016.

4. SMART, SAINT, and XPREP; Siemens Analytical X-ray Instruments Inc.: 1995.

5. G. M. Sheldrick, SADABS, Program for Area Detector Adsorption Correction; Institute for Inorganic Chemistry, University of Göttingen: 1996.

6. G. M. Sheldrick, Crystal structure refinement with SHELXL. Acta Crystallogr., Sect. C: Struct. Chem., 2015, 71, 3.

7. C. F. Macrae, I. Sovago, S. J. Cottrell, P. T. A. Galek, P. McCabe, E. Pidcock, M. Platings, G. P. Shields, J. S. Stevens, M. Towler and P. A. Wood, *J. Appl. Crystallogr*., 2020, **53**, 226.

8. J. Yoonus, R. Resmi and B. Beena, *Mater. Today: Proc*., 2021, **46**, 2969-2974.

9. K. Shimuraa and H. Yoshida, *Energy Environ. Sci*., 2011, **4**, 2467-2481.

10. A. Šulčius, *J. Sci. Educ*., 2008.

11. L. Rocchetti, A. Amato and F. Beolchini, *J. Clean. Prod*., 2016, **116**, 299-305.